

# Journal of Astronomical Telescopes, Instruments, and Systems

AstronomicalTelescopes.SPIEDigitalLibrary.org

## **Polarized beam patterns from a multimoded feed for observations of the cosmic microwave background**

Alan J. Kogut  
Dale J. Fixsen

**SPIE.**

Alan J. Kogut, Dale J. Fixsen, "Polarized beam patterns from a multimoded feed for observations of the cosmic microwave background," *J. Astron. Telesc. Instrum. Syst.* **4**(1), 014006 (2018), doi: 10.1117/1.JATIS.4.1.014006.

# Polarized beam patterns from a multimoded feed for observations of the cosmic microwave background

Alan J. Kogut<sup>a,\*</sup> and Dale J. Fixsen<sup>a,b</sup>

<sup>a</sup>Goddard Space Flight Center, Code 665, Greenbelt, Maryland, United States

<sup>b</sup>University of Maryland, College Park, Maryland, United States

**Abstract.** We measure linearly polarized beam patterns for a multimoded concentrator and compare the results to a simple model based on geometric optics. We convolve the measured copolar and crosspolar beams with simulated maps of cosmic microwave background (CMB) polarization to estimate the amplitude of the systematic error resulting from the crosspolar beam response. The uncorrected error signal has typical amplitude of 3 nK, corresponding to inflationary B-mode amplitude  $r \sim 10^{-3}$ . Convolution of the measured crosspolar beam pattern with maps of the CMB E-mode polarization provides a template for correcting the crosspolar response, reducing it to negligible levels. © The Authors. Published by SPIE under a Creative Commons Attribution 3.0 Unported License. Distribution or reproduction of this work in whole or in part requires full attribution of the original publication, including its DOI. [DOI: [10.1117/1.JATIS.4.1.014006](https://doi.org/10.1117/1.JATIS.4.1.014006)]

Keywords: beam pattern; polarimeter; cosmic microwave background.

Paper 17079 received Oct. 3, 2017; accepted for publication Jan. 22, 2018; published online Feb. 14, 2018.

## 1 Introduction

Linear polarization of the cosmic microwave background (CMB) provides a unique window into the physics of the early universe. Gravitational waves created during an inflationary epoch interact with the CMB at later times to impart a distinctive signature in linear polarization. For the simplest (single-field) inflation models, the amplitude of this B-mode signal depends on the energy scale of inflation as

$$E = 1.06 \times 10^{16} \left( \frac{r}{0.01} \right)^{1/4} \text{ GeV}, \quad (1)$$

where  $r$  is the power ratio of gravitational waves to density fluctuations.<sup>1</sup> Current measurements set upper limits  $r < 0.07$  at 95% confidence.<sup>2</sup> If inflation results from Grand Unified Theory physics (energy  $E \sim 10^{16}$  GeV), the B-mode amplitude should be of order 30 nK. Signals at this level could be detected by a dedicated polarimeter, providing a critical test of a central component of modern cosmology.

The inflationary signal is faint compared to the fundamental limit imposed by photon noise statistics for a single-moded detector in a one-second integration. Even ideal (noiseless) detectors suffer from this limit; the only solution is to collect more photons. The light-gathering ability of a detector can be specified by its etendue  $A\Omega$ , where  $A$  is the detector area and  $\Omega$  is the solid angle. Increasing the etendue adds modes, thereby increasing both the signal and the photon noise. The modes are independent, so that the noise increases as the square root of the etendue  $NEP \propto (A\Omega)^{1/2}$ . But since the signal increases linearly with etendue, the signal-to-noise ratio improves as  $(A\Omega)^{1/2}$ , increasing the overall system sensitivity.

A common implementation for CMB polarization increases the instrument etendue using a focal plane tiled with thousands of detectors (for a recent review, see Ref. 3). These systems typically couple the detector to the sky using optical structures (feed

horn, lenslet, phased antenna array), which restrict the system response to a single electromagnetic mode at the sensor. Single-moded systems achieve diffraction-limited angular resolution with well-defined (Gaussian) beam profiles, but the large number of sensors required drives system-level complexity and cost, both directly and through the accompanying need for cryogenic multiplexing to reduce the wire count to cold stages of the instrument.

Multimoded sensors provide an alternative design solution. The beam width of a diffraction-limited system observing a single polarization state in a single-mode scales with wavelength,  $A\Omega = \lambda^2$ . In a multimoded system, the etendue is fixed so that the number of modes scales as  $N_{\text{mode}} = A\Omega/\lambda^2$ . The different electromagnetic modes form an orthogonal basis set and add incoherently at the detector. Assuming nearly equal occupancy for most modes, the detector sensitivity then scales as  $N_{\text{mode}}^{1/2}$ . For detector area  $A \gg \lambda^2$ , the number of modes is large, allowing a corresponding reduction in detector count compared to a single-moded system of comparable sensitivity.

The primordial inflation explorer (PIXIE)<sup>4,5</sup> is a mission concept to measure CMB polarization at levels  $r < 10^{-3}$ . PIXIE combines four multimoded detectors with a polarizing Fourier transform spectrometer (FTS) to achieve background-limited sensitivity across a broad frequency range. Figure 1 shows the optical design. A pair of primary mirrors 55 cm in diameter produces two coaligned beams on the sky. Folding flats and secondary mirrors transfer the beams to the FTS, which mixes the beams and introduces an optical phase delay. The recombined beams are then routed to a pair of nonimaging concentrators, each of which contains two multimoded bolometric detectors to sense the fringe pattern as a function of optical phase delay. The instrument etendue of 400 mm<sup>2</sup> sr corresponds to flat-topped beam with full-width at half-maximum 2.6 deg on the sky, and is conserved throughout the optical path.

An important aspect of the proposed instrument design is the use of nonimaging concentrators to couple light from the FTS to the detectors. Each detector is sensitive to a single linear polarization; any crosspolar response to the orthogonal polarization

\*Address all correspondence to: Alan J. Kogut, E-mail, [alan.j.kogut@nasa.gov](mailto:alan.j.kogut@nasa.gov)

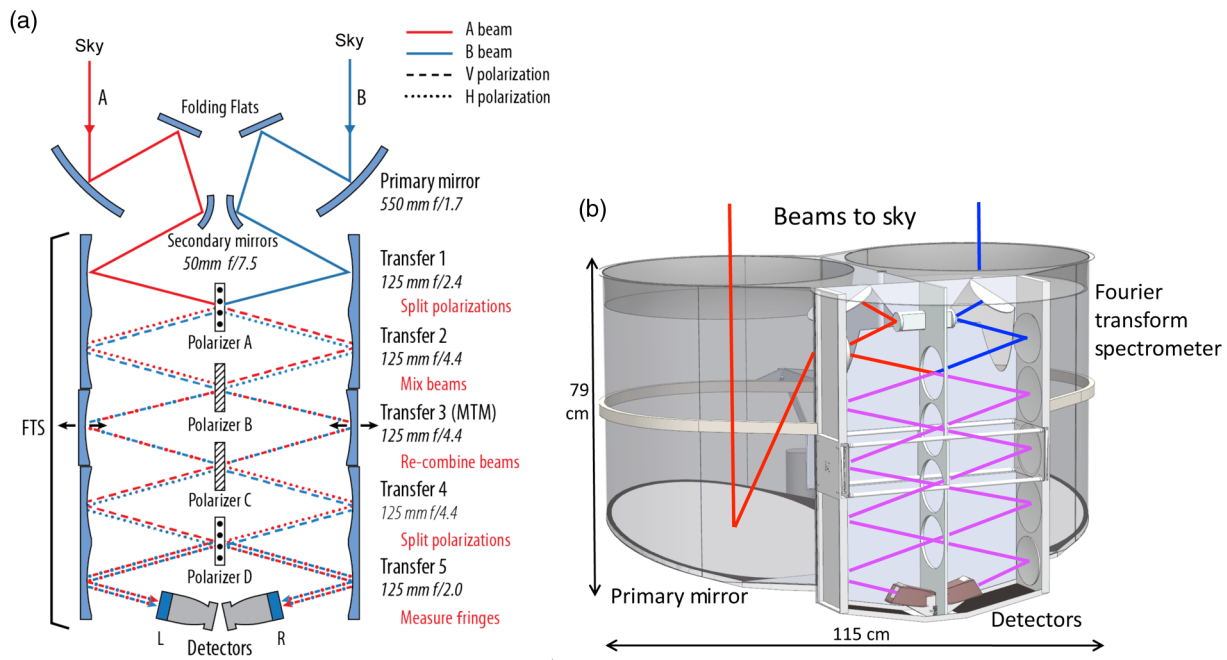


**Fig. 1** (a) Schematic view of the PIXIE optical signal path. A polarizing FTS interferes the signal from two copointed beams to produce a fringe pattern proportional to the difference spectrum between orthogonal polarization states from the two beams. Polarization-sensitive detectors mounted within multimoded concentrators sense the fringe pattern. (b) Physical layout of PIXIE optics.

produces an effective rotation of the measured polarization with respect to the true polarization on the sky. The crosspolar response of single-moded structures is well understood. A corrugated circular feedhorn, for example, will typically exhibit crosspolarization at levels  $-25$  dB with a distinctive quadrupolar (cloverleaf) angular pattern.<sup>6</sup> The crosspolar response of multimoded structures is more complicated. We describe measurements and modeling of the copolar and crosspolar beam patterns for a rectangular multimoded concentrator designed for the PIXIE polarimeter and assess the impact of the measured crosspolar response for measurements of the inflationary polarization signal.

## 2 Multimoded Concentrator Design

Figure 2 shows the concentrator design, which transforms the  $f/2$  beam from the FTS to a  $2\pi$  sr solid angle at the detector.

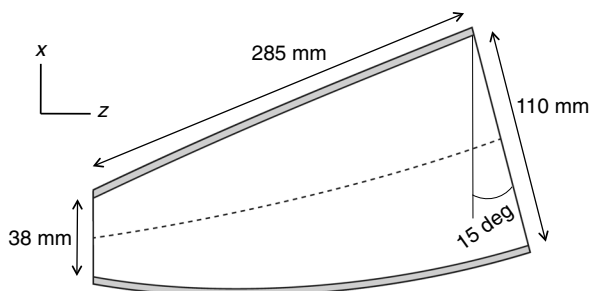


**Fig. 2** Schematic of the rectangular concentrator in the  $\hat{x} - \hat{z}$  plane. The dashed line indicates the junction of the  $\hat{u}$  and  $\hat{v}$  walls, which project out of the plane of the page (see text). Dimensions are for the larger scaled concentrator used to measure the beam patterns; the concentrator for the actual instrument is three times smaller in all dimensions.

To preserve linear polarization, the concentrator has a rectangular cross section, with four walls each of which forms an elliptical section. Each concentrator contains a pair of polarization-sensitive bolometers, mounted within an integrating cavity at the exit aperture of the concentrator. Each bolometer detects a single linear polarization; the pair is mounted with their polarization directions rotated by 90 deg to measure orthogonal polarization states.

Light from the FTS enters the concentrator at an angle of 15 deg from the  $\hat{z}$  axis. The concentrator design minimizes the resulting asymmetry in the polarized beam patterns by rotating the concentrator 45 deg about the  $\hat{z}$  axis. Since the instrument remains symmetric from side to side ( $-\hat{y}$  to  $+\hat{y}$ ), the rotated concentrator has two identical “top” walls and two

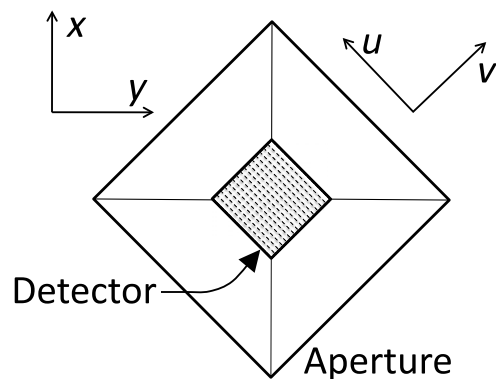


**Fig. 3** Schematic view looking into the concentrator aperture from the FTS, showing the instrument ( $xy$ ) and concentrator ( $uv$ ) coordinate systems. The concentrator is rotated 45 deg with respect to instrument coordinates so that asymmetries in instrument coordinates affect both detectors equally. Dashed lines show the orientation of the absorbing grid for the  $\hat{u}$  detector.

identical “bottom” walls, with the top and bottom figures described by different elliptical sections. The detectors are mounted behind the square exit aperture formed by the four walls and are necessarily aligned with the concentrator walls. In terms of the instrument coordinate system, we may write the detector polarizations as

$$\hat{u} = \frac{\hat{x} - \hat{y}}{\sqrt{2}} \quad \hat{v} = \frac{\hat{x} + \hat{y}}{\sqrt{2}}, \quad (2)$$

with one detector sensitive to  $\hat{u}$  rotated 45-deg counterclockwise from the vertical ( $+\hat{x}$ ) and the other sensitive to  $\hat{v}$  rotated 45-deg clockwise (Fig. 3). Since the detector  $[uv]$  coordinates are symmetric with respect to any top–bottom ( $\hat{x}$ ) asymmetry, the polarized beam patterns from the detector pair are correspondingly

**Table 1** Measurement frequencies and number of modes.

Measurement frequency (GHz)	Sky frequency (GHz)	Number of modes $N_{\text{mode}}$
10.8	32	5
35	105	49
91	273	330

symmetric. (A previous version<sup>7</sup> of the concentrator did not employ this 45-deg rotation and had a poorer match between the beams.)

### 3 Polarized Beam Pattern Measurements

We measured the copolar and crosspolar beam patterns of a scaled version of the PIXIE concentrator. Measurements took place within the Goddard Electromagnetic Anechoic Chamber (GEMAC) facility and are similar to previous measurements described in Ref. 7. Briefly, we transmit power in a single linear polarization and use an unpolarized Thomas Keating THz absolute power meter to record the power at the concentrator as a function of angle from the point-source transmitter. A wire grating between the power meter and the exit aperture of the concentrator defines the polarization state at the power meter. The grating can be rotated to sample either the  $\hat{u}$  or  $\hat{v}$  polarization. An absorbing iris at entrance aperture of the concentrator truncates the corners of the aperture and serves as a beam stop to circularize the beam patterns.

Although PIXIE’s FTS has frequency response to THz frequencies, the fixed noise of the power meter and the limited broadcast power available at frequencies above 100 GHz make direct measurements at higher frequencies impractical. Instead, we increase all dimensions of the PIXIE concentrator by a factor of three and measure the beam patterns of the scaled

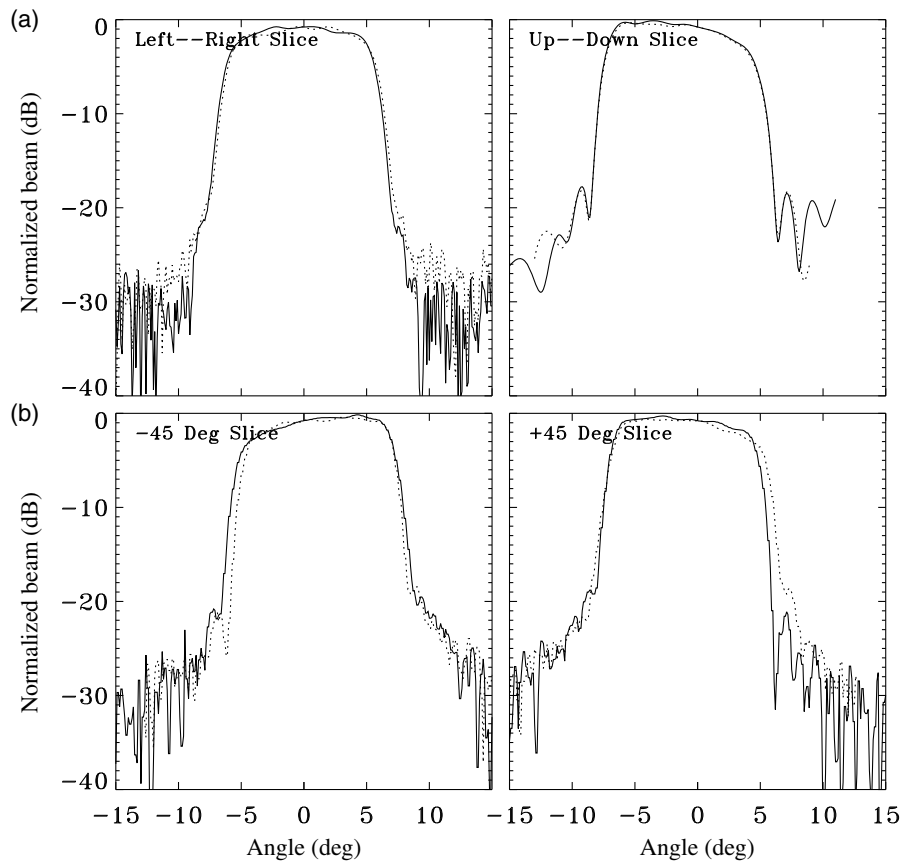


**Fig. 4** Comparison of copolar beam patterns for  $\hat{u}$  (solid line) and  $\hat{v}$  (dotted) polarization measured at 35 GHz for the scaled concentrator. Four slices through the flat-topped two-dimensional beam pattern are shown. (a) Up–down and left–right slices correspond to slices oriented along the instrument  $\hat{x}$  and  $\hat{y}$  coordinates. (b) –45 deg and +45 deg slices correspond to the detector  $\hat{u}$  and  $\hat{v}$  coordinate directions (see Figure 1). Mounting the concentrator at a 45-deg angle produces nearly identical beam patterns for both detector polarizations.

concentrator at frequencies 10.8, 35, and 91 GHz corresponding to sky measurements of 32, 105, and 273 GHz for the unscaled concentrator. The frequencies are selected to measure the beam pattern in the few-mode limit, the multimoded geometric optics limit, and an intermediate case (Table 1). Note that the frequency spectrum of the CMB polarization follows the derivative  $\text{dB}/\text{dT}$  of a blackbody spectrum and peaks at frequencies near 270 GHz well into multimoded operation. GEMAC data at 91 GHz sample the beam pattern near this peak.

The measured beam patterns include the response of the concentrator as well as the detector. The PIXIE detectors use silicon wires degeneratively doped with phosphorus to absorb light in a single linear polarization.<sup>8</sup> The measured beam patterns use a wire grating to reflect light in a single linear polarization, then measure the transmitted light in the orthogonal polarization using an unpolarized power meter. The geometry of the power meter aperture and its location within the integrating cavity, as well as the position of the reflective wire grating, are appropriately scaled to match the detector for the PIXIE FTS.

Figure 4 shows the copolar beam patterns measured at 35 GHz with the scaled concentrator (corresponding to 105 GHz for the unscaled design). Figure 4(a) shows slices through the flat-topped beam in the left–right (instrument  $+\hat{y}$  to  $-\hat{y}$ ) and up–down (instrument  $+\hat{x}$  to  $-\hat{x}$ ) directions. As expected, the beam patterns are symmetric with respect to  $\hat{y}$  but show a few-dB “tilt” in  $\hat{x}$  from the off-axis illumination. Figure 4(b) shows the beam patterns along  $-45$  deg and  $+45$  deg slices correspond to the detector  $\hat{u}$  and  $\hat{v}$  coordinate directions.

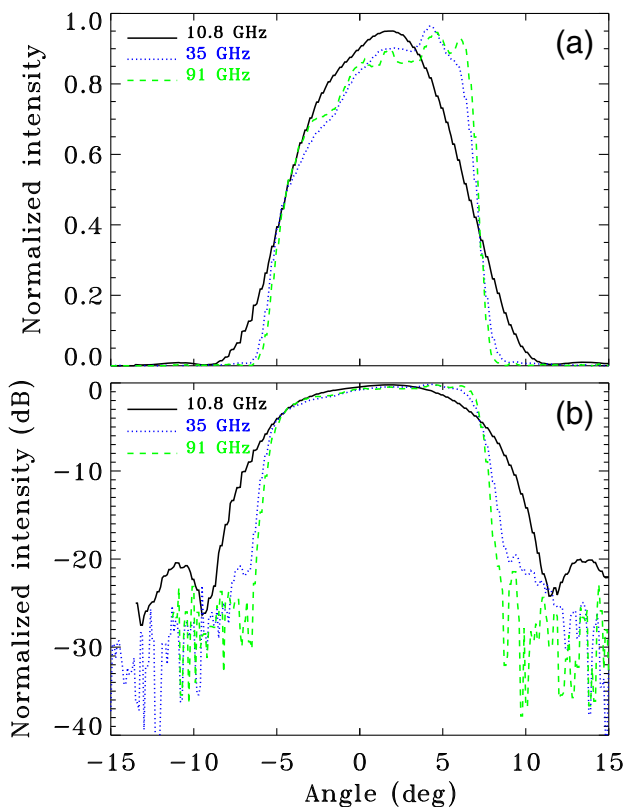


**Fig. 5** Comparison of copolar beam patterns as a function of frequency for the  $\hat{u}$  polarization along the  $+45$  deg slice. Beam patterns are shown for both (a) a linear scale and (b) logarithmic scale. Diffraction broadens the beam pattern at the lowest frequency, but the beam shape is nearly constant at higher frequencies.

Note that for all four slices, the copolar beam pattern sampled by the  $\hat{u}$  detector is nearly identical to the pattern sampled by the orthogonal  $\hat{v}$  detector. This minimizes temperature–polarization mixing between unpolarized (temperature) gradients and the smaller polarized sky signal.

Figure 5 compares a slice through the copolar  $\hat{u}$  beam in the  $\hat{u}$  orientation at each of the mapped frequencies. The beam profile is similar at 35 and 91 GHz but broadens at 10.8 GHz where diffraction plays a more significant a role.

The copolar beam patterns measure the response of the concentrator to a linearly polarized plane wave, when the polarization of the incident beam matches the polarization accepted by the detector (e.g.,  $\hat{u}$  incident polarization measured by the  $\hat{u}$  detector). We also measure the crosspolar response when the detector is orthogonal to the incident polarization ( $\hat{u}$  incident polarization measured by the  $\hat{v}$  detector). Figure 6 shows the crosspolar beam pattern measured at 35 GHz. As with Fig. 4, we show the crosspolar response in four slices through the flat-topped beam, corresponding to the principal instrument ( $\hat{x}$  and  $\hat{y}$ ) and detector ( $\hat{u}$  and  $\hat{v}$ ) symmetries.

The crosspolar beam pattern has a similar flat-topped shape as the copolar beam but at a reduced amplitude. The dominant effect of the crosspolar response is a modest reduction in polarization efficiency (Table 2). The measured beam patterns correspond to polarization efficiency of  $\sim 0.95$ , nearly independent of frequency. The polarization efficiency reduces the instrument response to a linearly polarized sky signal, and may be absorbed into the instrument calibration. It thus affects instrument signal-to-noise estimates but does not induce systematic error in the measured sky polarization.

## 4 Comparison with Model

We model the copolar and crosspolar beam patterns using a ray-trace code in the geometric optics limit. As discussed in Ref. 7, we account for operation in the few-mode limit by first binning the modeled beam pattern on a rectangular grid, Fourier transforming the binned beam map, sorting the complex Fourier coefficients by angular frequency, and Fourier transforming back to real space using only the lowest  $N_{\text{mode}}$  values. This removes the high spatial frequency information from the modeled beam pattern, approximating the effect of few-mode operation without computationally expensive phase matching. We then convolve the mode-truncated pattern with the Airy pattern for the appropriate observing frequency to approximate the effects of diffraction at the iris.

Figure 7 compares the copolar and crosspolar beam patterns at measured frequency 35 GHz. Data and model agree well across the flat-topped beam, with rms difference 0.7 dB in both the copolar and crosspolar response for either  $\hat{u}$  or  $\hat{v}$  polarization. The agreement between the measured and modeled beam patterns highlights the utility of the simple model technique. Direct electromagnetic computation of beam patterns through software code, such as CST or HFSS requires amplitude and phase matching for each mode. A large number of modes in an off-axis geometry require long computational times for a single configuration, becoming prohibitive for a design process with multiple iterations. The ray-trace code is simple, fast, and readily accounts for effects including off-axis orientation and complex detector geometries while retaining accurate modeling of both the copolar and crosspolar beam response.

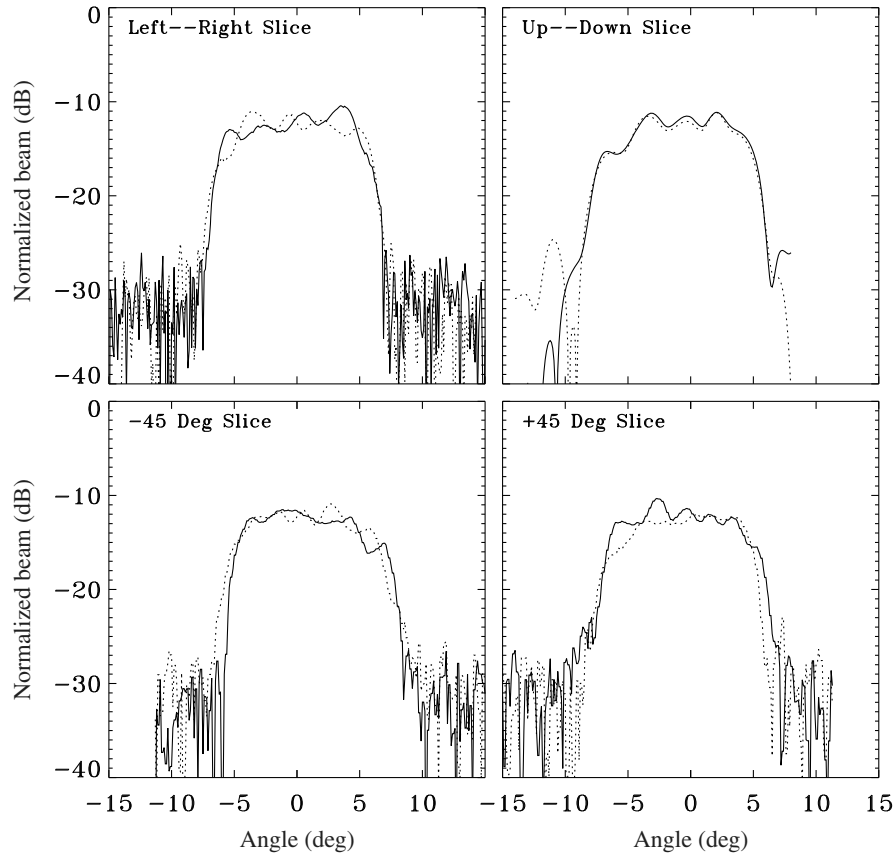


**Fig. 6** Comparison of crosspolar beam patterns for  $\hat{u}$  (solid line) and  $\hat{v}$  (dotted) polarization measured at 35 GHz for the scaled concentrator. Beam slices are the same as Fig. 4.

**Table 2** Polarization efficiency.

Measurement frequency (GHz)	Polarization efficiency
10.8	0.96
35	0.93
91	0.95

## 5 Discussion

Each PIXIE detector samples a single linear polarization (Stokes  $Q$  in instrument-fixed coordinates). The instrument rotates about the beam boresight to modulate the sky signal, allowing reconstruction of Stokes  $Q$  and  $U$  parameters for each independent pixel on the sky.<sup>4</sup> Structure within the crosspolar response on angular scales smaller than the beam width can generate systematic error in the reconstructed sky signal. We estimate the magnitude of this effect by convolving the measured copolar

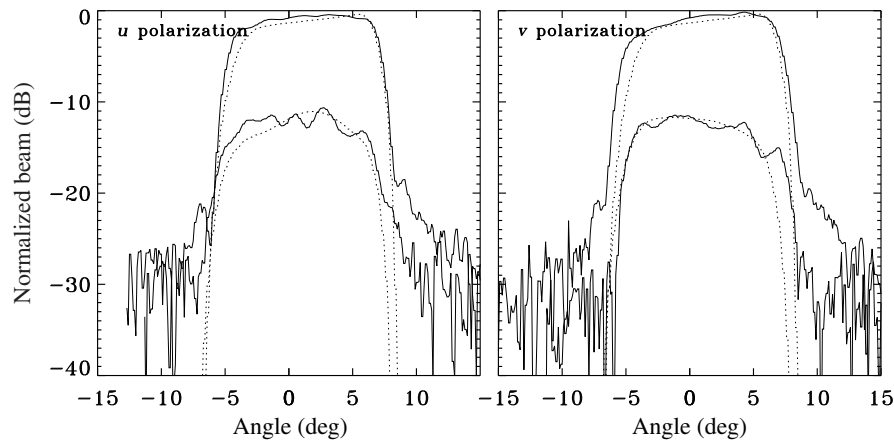


**Fig. 7** Comparison of measured beam patterns at 35 GHz (solid lines) to the model including effects of diffraction and the number of modes (dotted lines). The upper set of curves show the copolar beam while the lower set shows the crosspolar response. The primary effect of the crosspolar response is a 5% loss in polarization efficiency.

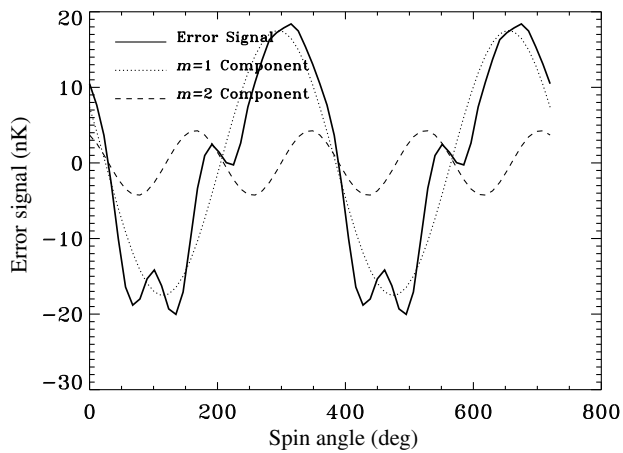


**Fig. 8** Systematic error for the 35-GHz crosspolar response convolved with simulated CMB maps. The crosspolar response (solid line) is dominated by an  $m = 1$  dipole component (dotted line), which does not contribute to the reconstructed sky polarization. The  $m = 2$  component (dashed line) creates a systematic error in polarization, but is small compared to the  $r = 0.01$  inflationary signal.

and crosspolar beam patterns with Monte Carlo simulations of polarized CMB sky signals.

The beam patterns for the full PIXIE instrument depend on both the concentrator and the fore-optics. Ray-trace modeling shows that the crosspolar response is dominated by the concentrator. We thus use the beam patterns measured for the scaled concentrator to estimate the systematic error resulting from the crosspolar beam response of the full instrument. The concentrator is designed to illuminate the transfer mirror T5 coupling the detectors to the spectrometer. The measured beam widths of the concentrator thus do not represent the width of the final PIXIE beams on the sky. However, since the optics conserve beam etendu, we may approximate the final beam on the sky by scaling the measured copolar and crosspolar beam patterns by the diameter ratio of the 112-mm coupling mirror used for beam measurements to the PIXIE 550 mm primary mirror. The resulting beam has a diameter of 2.6 deg.

We generate random realizations of CMB polarization using a standard  $\Lambda$ CDM cosmology,<sup>9</sup> evaluated to harmonic moment  $\ell = 1500$  (angular scale 7 in.). We convolve the simulated Stokes  $Q$  and  $U$  maps with the scaled beam to generate the instrument response at fixed spin angle  $\gamma$ , then rotate the beam with respect to the sky and repeat for 32 angular steps uniformly covering spin angle  $[0, 2\pi]$ . Although the PIXIE fore-optics and FTS interfere the signals from two copointed beams, we ignore any additional cancellation of beam effects from the fore-optics and simply scale the beam patterns measured from the concentrator. The resulting signal is thus an upper limit to the systematic error expected from the full PIXIE optical system.

Figure 8 shows the resulting systematic error signal for two complete rotations of the beam over the simulated sky. The solid line shows the effect of the crosspolar response of the scaled 35-GHz beam (corresponding to 105 GHz sky signal). The “tilt” in the beam from the off-axis illumination modulates the response at the spin period. Since a true polarization signal is modulated twice per spin, the tilt does not contribute to the reconstructed polarization. We fit the simulated data to azimuthal spin modes

$$T(\gamma) = \sum_m [a_m \cos(m\gamma) + b_m \sin(m\gamma)], \quad (3)$$

where  $m$  denotes the azimuthal order. The dotted line shows the dipole ( $m = 1$ ) component. The  $m = 2$  component (dashed line) is degenerate with true sky polarization but is substantially smaller. We repeat the analysis for 100 realizations of the CMB sky. The  $m = 2$  systematic error component has mean amplitude  $\langle (a_2^2 + b_2^2)^{1/2} \rangle = 3.3$  nK with standard deviation 1.7 nK. Compared to the inflationary B-modes, the  $m = 2$  error from the measured crosspolar response corresponds to mean  $r = 1.2 \times 10^{-3}$  with standard deviation  $r = 0.6 \times 10^{-3}$ . Note that this represents an upper limit to the potential systematic error before correction. CMB polarization is dominated by the E-mode component. The measured crosspolar beam pattern may be convolved with maps of the E-mode polarization to correct the crosspolar response, further reducing its effect on B-mode searches.

## 6 Conclusion

We measure the copolar and crosspolar beam patterns from a multimoded concentrator designed for the PIXIE polarimeter. The beams provide a flat-topped pattern on the sky and are fully symmetrized between orthogonal linear polarizations. The crosspolar beam pattern has similar angular dependence as the copolar beam; the dominant effect of the crosspolar response is a reduction in polarization efficiency to a measured efficiency of 95%. Structure in the crosspolar response on angular scales smaller than the 2.6-deg copolar beam creates a systematic error when reconstructing the polarization signal from the sky. Monte Carlo simulations show the uncorrected error signal to have mean amplitude  $3.3 \pm 1.7$  nK, corresponding to an error  $\delta r = [1.2 \pm 0.6] \times 10^{-3}$  for the inflationary B-mode signal. Convolution of the measured crosspolar beam pattern with maps of the CMB E-mode polarization provides a template for correcting the crosspolar response, reducing it to negligible levels.

## Acknowledgments

The authors gratefully acknowledge the assistance of G. De Amici and S. Seufert for measurements of the polarized beam patterns.

## References

1. D. H. Lyth and A. Riotto, “Particle physics models of inflation and the cosmological density perturbation,” *Phys. Rep.* **314**, 1–146 (1999).
2. P. A. R. Ade et al., “Improved constraints on cosmology and foregrounds from BICEP2 and Keck array cosmic microwave background data with inclusion of 95 GHz band,” *Phys. Rev. Lett.* **116**, 031302 (2016).
3. M. H. Abitbol et al., “*CMB-S4 Technology Book*, 1st ed.,” ArXiv e-prints arXiv:1706.02464 (2017).
4. A. Kogut et al., “The primordial inflation explorer (PIXIE): a nulling polarimeter for cosmic microwave background observations,” *J. Cosmol. Astropart. Phys.* **2011**, 025 (2011).
5. A. Kogut et al., “The primordial inflation explorer (PIXIE),” *Proc. SPIE* **9904**, 99040W (2016).
6. P. Kildal, *Foundations of Antennas: A Unified Approach*, Professional Publishing Service, Berlin, Connecticut (2000).
7. A. Kogut, D. J. Fixsen, and R. S. Hill, “Polarization properties of a broadband multi-moded concentrator,” *J. Opt. Soc. Am. A* **32**, 1040 (2015).
8. P. C. Nagler et al., “Multimode bolometer development for the PIXIE instrument,” *Proc. SPIE* **9914**, 99141A (2016).
9. P. A. R. Ade et al., “Planck 2015 results. XIII. Cosmological parameters,” *Astron. Astrophys.* **594**, A13 (2016).

**Alan J. Kogut** is an astrophysicist at NASA's Goddard Space Flight Center. He received his AB from Princeton University and his PhD from the University of California at Berkeley. His research focuses on observations of the frequency spectrum and linear polarization of the cosmic microwave background and diffuse astrophysical foregrounds at millimeter and sub-mm wavelengths.

**Dale J. Fixsen** is an astrophysicist at the University of Maryland. He received his BS from Pacific Lutheran University, Tacoma, Washington, and his PhD from Princeton University. His research focuses on the spectrum, temperature, and polarization of the cosmic microwave background and the radio and infrared cosmic backgrounds.